NANO LETTERS

Letter

pubs.acs.org/NanoLett

Unravelling the Roles of Size, Ligands, and Pressure in the Piezochromic Properties of CdS Nanocrystals

Niccolò R. C. Corsini,[†] Nicholas D. M. Hine,[§] Peter D. Haynes,[†,‡] and Carla Molteni*[,∥]

[†]Department of Physics and [‡]Department of Materials, Imperial College London, Exhibition Road, London SW7 2AZ, U.K.
[§]Department of Physics, University of Warwick, Coventry CV4 7AL, U.K.
[∥]Department of Physics, King's College London, Strand, London WC2R 2LS, U.K.

Supporting Information

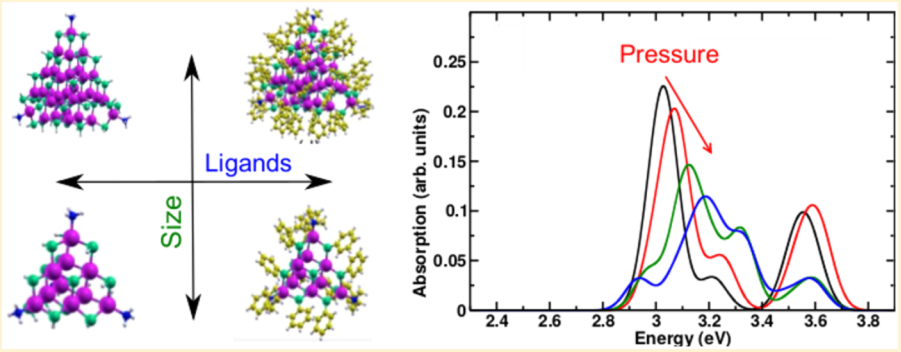

ABSTRACT: Understanding the effects of pressure-induced deformations on the optoelectronic properties of nanomaterials is important not only from the fundamental point of view but also for potential applications such as stress sensors and electromechanical devices. Here, we describe the novel insights into these piezochromic effects gained from using a linear-scaling density functional theory framework and an electronic enthalpy scheme, which allow us to accurately characterize the electronic structure of CdS nanocrystals with a zincblende-like core of experimentally relevant size. In particular, we focus on unravelling the complex interplay of size and surface (phenyl) ligands with pressure. We show that pressure-induced deformations are not simple isotropic scaling of the original structures and that the change in HOMO−LUMO gap with pressure results from two competing factors: (i) a bulk-like linear increase due to compression, which is offset by (ii) distortions and disorder and, to a lesser extent, orbital hybridization induced by ligands affecting the frontier orbitals. Moreover, we observe that the main peak in the optical absorption spectra is systematically red-shifted or blue-shifted, as pressure is increased up to 5 GPa, depending on the presence or absence of phenyl ligands. These heavily hybridize the frontier orbitals, causing a reduction in overlap and oscillator strength, so that at zero pressure, the lowest energy transition involves deeper hole orbitals than in the case of hydrogen-capped nanocrystals; the application of pressure induces greater delocalization over the whole nanocrystals bringing the frontier hole orbitals into play and resulting in an unexpected red shift for the phenyl-capped nanocrystals, in part caused by distortions. In response to a growing interest in relatively small nanocrystals that can be difficult to accurately characterize with experimental techniques, this work exemplifies the detailed understanding of structure−property relationships under pressure that can be obtained for realistic nanocrystals with state-of-the-art first-principles methods and used for the characterization and design of devices based on these and similar nanomaterials.

KEYWORDS: *II−VI nanocrystals, piezochromic properties, linear scaling methods, electronic enthalpy, time-dependent density functional theory*

Group II−VI nanocrystals, such as CdS and CdSe, have received much attention due to their optical properties, colloidal processability, and stability under a wide range of operating conditions.[1] The dependence of nanocrystal optical and electronic properties on pressure, and how this dependence varies with size and surfactants, is still very much an open question. Defects also affect the mechanical properties of nanomaterials.[2] This is not only of fundamental interest but also has technological importance for applications such as nanoscale stress sensors and other tunable optoelectronic and electromechanical devices.[3,4] Organic ligands with large HOMO−LUMO gaps are often used to passivate nanocrystal surfaces and saturate dangling bonds. The impact of ligands on nanocrystal properties goes beyond simple passivation[5] and can be used to functionalize and modulate their chemophysical properties in a variety of ways: increase their solubility, prevent

Received: October 25, 2016
Revised: January 22, 2017
Published: January 27, 2017

DOI: 10.1021/acs.nanolett.6b04461
Nano Lett. 2017, 17, 1042−1048

nanocrystal agglomeration and corrosion,[6] and tune band-edge energy levels[7] and optical properties.[8] Progress in the synthesis and demands from applications are driving research toward nanocrystals of increasingly smaller size, where surface effects become important. Although these systems pose a challenge to experimental characterization techniques, they are approaching sizes that are treatable with state-of-the-art first-principles electronic structure calculations, which can provide precise insight into their optoelectronic properties, unravel competing effects, and guide the design of novel and tunable nanosystems. While force-field-based simulations have provided interesting insights into structural-transformation mechanisms in semiconductor nanocrystal under pressure,[9−13] first-principles calculations of nanocrystals under pressure have been limited so far to very small systems.[14−20]

Here, we present the results of a series of computational experiments, within a linear-scaling density-functional theory (DFT) framework, which aim to explore the piezochromic properties (i.e., the optoelectronic response under pressure) of prototypical realistic CdS nanocrystals. The goal of our simulations is to disentangle, at the atomic and the electronic levels, the effects of pressure, size, and surface ligands, which would be difficult to separate in experiments. We focus on $Cd_{32}S_{14}(SC_6H_5)_{36}\cdot 4(N(CH_3)_3)$, as well as the hydrogen-capped $Cd_{32}S_{14}(SH)_{36}\cdot 4NH_3$, and their smaller versions (with similar shape and stoichiometry) $Cd_{10}S_4(SC_6H_5)_{12}\cdot 4(N(CH_3)_3)$ and $Cd_{10}S_4(SH)_{12}\cdot 4NH_3$. These are, respectively, referred to as $[CdS]_{32}$−Ph, $[CdS]_{32}$−H, $[CdS]_{10}$−Ph, and $[CdS]_{10}$−H in the following. Their structures are shown in Figure 1 and allow us

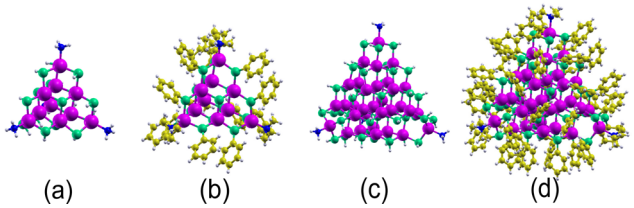

Figure 1. Simulated CdS nanocrystal structures: (a) $Cd_{10}S_4(SH)_{12}\cdot 4NH_3$ ($[CdS]_{10}$−H), (b) $Cd_{10}S_4(SC_6H_5)_{12}\cdot 4(N(CH_3)_3)$ ($[CdS]_{10}$−Ph), (c) $Cd_{32}S_{14}(SH)_{36}\cdot 4NH_3$ ($[CdS]_{32}$−H), and (d) $Cd_{32}S_{14}(SC_6H_5)_{36}\cdot 4(N(CH_3)_3)$ ($[CdS]_{32}$−Ph).

to carefully unravel the influence of size and ligands. We do not address in this study the effects of different shapes, which may be important especially for very small nanocrystals. We choose $[CdS]_{32}$−Ph because it is chemically analogous to $Cd_{32}S_{14}(SC_6H_5)_{36}(DMF)_4$ (where DMF refers to *N*,*N*-dimethylformamide), a nanocrystal with an 82 atoms zincblende (ZB) core, which has been synthesized through crystallization of nanocrystals into superlattices[21] and has a well-characterized single-sized structure; it has the benefit of having been studied experimentally, including under pressure.[22] It has a substantial crystalline core while being sufficiently small (530 atoms) to be treated by first-principles methods and will serve as a benchmark.

To simulate the CdS nanocrystals under pressure, we use an electronic enthalpy scheme,[18,19] in which the nanocrystal excluded volume in the pressure × volume term in the enthalpy is defined as that enclosed within an electronic density isosurface, which can efficiently handle complex shapes such as the intricate ones that characterize the phenyl-capped CdS systems. This scheme models a nanocrystal immersed in an implicit pressure transmitting medium, of which it provides a homogeneous and time-averaged description (as opposed to methods considering explicit media).[12] The emphasis is laid on the role played by electrons as pressure mediators as pressure is applied normal to the electronic density isosurface, whose isovalue needs to be appropriately tuned.[19] While this scheme can also be used at finite temperature with increased computational costs, we use it to optimize quasi-statically the nanocrystals structures and obtain the minimum enthalpy configuration at a given pressure. Here we are interested in a deformation rather than a phase-transformation regime, as relevant, e.g., for stress sensors. While the most-significant results are those in the range 0−5 GPa, we overpressurize (and consequently overdeform) the nanosystems up to larger values (15 GPa, which are included for completeness) than those at which structural transformations would occur experimentally.[22] To simulate structural transformations at realistic pressures, thermal effects and enhanced sampling would need to be included. In contrast with the hydrogen-capped cluster, the introduction of explicit phenyl ligands induces some disorder and, hence, lifts degeneracies in the electronic energy levels; these disorder effects are captured even with simple geometry optimization. For the optical absorption spectra, we use the linear-response time-dependent DFT (TDDFT) formalism[23] within the Tamm−Dancoff approximation and mimic broadening thermal effects with a Gaussian smearing of 0.05 eV. Both the electronic enthalpy method and TDDFT were recently implemented in the linear-scaling DFT code ONETEP.[19,24−28] We perform all calculations within Blöchl's projector-augmented wave (PAW) formalism,[29,30] particularly useful to efficiently describe Cd, the PW92 local density approximation (LDA) exchange-correlation functional,[31] an 800 eV equivalent plane-wave cutoff, and two minimal sets of local orbitals optimized in situ separately for the occupied and unoccupied subspaces,[25] with localization radii of 4.8 and 6.3 Å, respectively. Although LDA is known to underestimate energy gaps and may inaccurately describe some charge-transfer effects in TDDFT,[32] our simulation setup is validated on available experimental data and allows us to capture qualitative trends for the selected complex nanocrystals that would not be computationally tractable with more sophisticated methods including, e.g., range-separated exchange-correlation functionals with a fraction of exact exchange.[33] Further computational details and benchmarking tests are available in the Supporting Information.

The fully relaxed nanocrystals' geometries under pressure demonstrate that the pressure dependence of the bond strain pattern cannot be represented by an isotropic scaling of atomic coordinates dictated by the bulk modulus, as it is often assumed.[20,34,35] Crucially, the electronic enthalpy method we employ allows for anisotropic pressure-dependent structural relaxation. This is exemplified by Figure 2, which shows, for $[CdS]_{32}$−Ph, a complex pattern of Cd−S bond contraction and dilation as a function of the distance from the surface.

Even at the center of the nanocrystal, the bonds are compressed well beyond the bulk ZB values, so we should not assume that the core is perfectly bulk-like. $[CdS]_{32}$−Ph at 0 GPa has an average Cd−S bond length of 2.501 Å, in excellent agreement with the experimental value of 2.503 Å for $Cd_{32}S_{14}(SC_6H_5)_{36}(DMF)_4$ at 6.5 K.[21] The bond strain pattern is strongly dependent on the size and on the ligands. In fact, a smaller size and phenyl ligation increase the spread of Cd−S bond lengths for both a given shell and shell distance from the nanocrystal center (see the Supporting Information). This

DOI: 10.1021/acs.nanolett.6b04461
Nano Lett. 2017, 17, 1042−1048

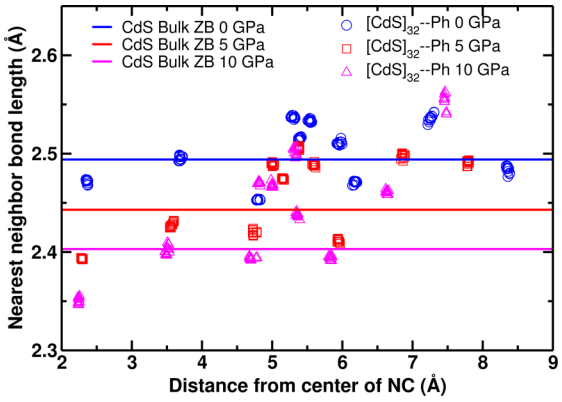

Figure 2. Distribution of nearest neighbor Cd−S distances as a function of the distance from the center of the nanocrystal (NC) for $[CdS]_{32}$−Ph at 0, 5, and 10 GPa with the corresponding bulk zincblende (ZB) values for reference.

indicates that the nanocrystal deforms differently depending on the size and ligands, which can be attributed to differences in surface energy and ligand-surface interactions.

Size and ligands have a strong impact on structural as well as optoelectronic properties of nanocrystals under pressure. Figure 3 shows the behavior of HOMO−LUMO gaps with pressure for the different nanocrystals and compares it to the values for bulk ZB and wurtzite (WZ, the stable structure at ambient conditions), for which experimental data are available, including the phase transition to rocksalt (RS)[36]. In the absence of phase transitions, bulk CdS has an optical gap that varies linearly with pressure, while nanocrystals can display nonlinear and qualitatively different behavior.

The HOMO−LUMO gap of $[CdS]_{32}$−H increases linearly between 0 and 5 GPa with a gradient of 28 meV/GPa compared to 30 meV/GPa for bulk ZB simulated with DFT; however, above 5 GPa, the energy gap of $[CdS]_{32}$−H is found to decrease as the distortions become important and reduces by 0.43 eV when overpressurized from 0 to 15 GPa. In contrast to $[CdS]_{32}$−H, $[CdS]_{32}$−Ph deviates from the bulk-like behavior at smaller pressures due to the more pronounced ligand-induced distortions. This behavior is amplified for $[CdS]_{10}$−H and $[CdS]_{10}$−Ph because of the smaller size and prominence of surface energetics, with the HOMO−LUMO gap of $[CdS]_{10}$−H hardly changing and that of $[CdS]_{10}$−Ph decreasing over the tested pressure range. The almost constant trend of the HOMO−LUMO gap of $[CdS]_{10}$−H with pressure is due to the fact that increased disorder and distortion with respect to its larger counterpart induce a decrease of the HOMO−LUMO gap with pressure that compensates the bulk-like linear increase.

The rich phenomenology of the simulated nanocrystals under pressure is the result of a complex interplay between geometry and electronic structure. We investigate the band edge orbitals to gain further insight. Figure 3 shows the features of HOMO and LUMO for $[CdS]_{32}$−H and $[CdS]_{32}$−Ph before applying pressure. The HOMO belongs to a set of three degenerate π-orbitals delocalized over the whole nanocrystal (HOMO−2−HOMO) but with more weight on S atoms. The LUMO, instead, is a midgap state typical of nonstoichiometric anion-rich ionic nanocrystals,[37] as can be seen in the electronic density of states (DOS) in Figure 4. The LUMO is also delocalized over the whole nanocrystal but with relatively more weight on the Cd atoms. The ordering and character of the band edge orbitals remains largely unchanged going from 0 to 5 GPa (see the Supporting Information). $[CdS]_{10}$−H has similar, albeit less-symmetric, orbitals compared to $[CdS]_{32}$−H: they appear to distort more strongly with pressure, which explains why the trends of the energy gap differ more substantially from the bulk-like behavior of $[CdS]_{32}$−H up to 5 GPa, confirming the compensating effects on the HOMO−LUMO gap between disorder and distortion and isotropic bulk-like compression (see the Supporting Information). Figure 3 shows that for $[CdS]_{32}$−Ph, the HOMO and LUMO are similar in character to the $[CdS]_{32}$−H equivalents, except that they are to some extent delocalized over both core and phenyl surfactants, especially the HOMO, in agreement with the experimental observation that phenyl rings act as good hole acceptors; the HOMO is localized more strongly over surface S atoms and phenyl, while the LUMO is more evenly distributed over both Cd and S in the core and less delocalized over the phenyl rings.

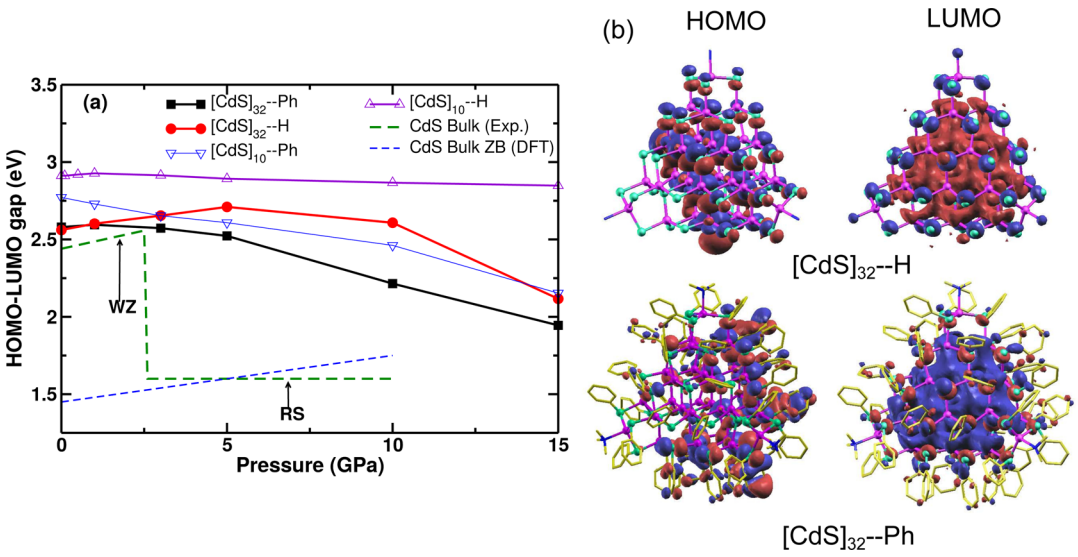

Figure 3. (a) Pressure dependence of HOMO−LUMO gaps for the nanocrystals and zincblende (ZB) and wurtzite (WZ) bulk crystals (DFT and experiments).[36] (b) HOMO and LUMO orbitals (0.01 $Å^{-3/2}$ orbital density isosurface) for $[CdS]_{32}$−H and $[CdS]_{32}$−Ph.

DOI: 10.1021/acs.nanolett.6b04461
Nano Lett. 2017, 17, 1042−1048

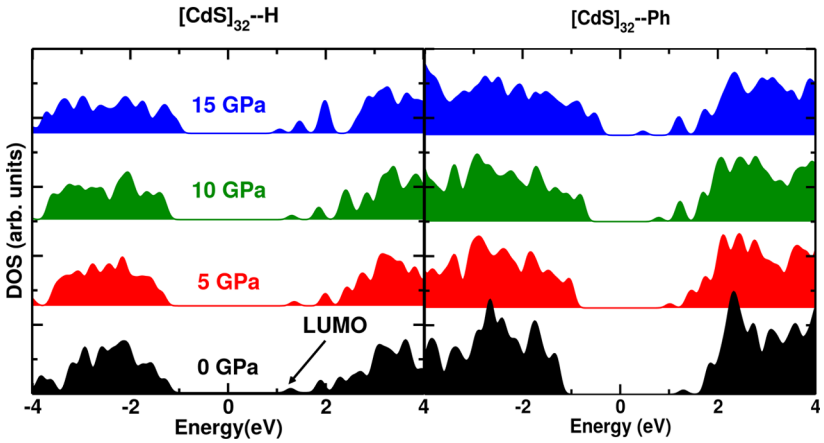

Figure 4. Electronic density of states of $[CdS]_{32}$−H (left) and $[CdS]_{32}$−Ph (right) at 0, 5, 10, and 15 GPa.

Increasing pressure from 0 to 5 GPa has the effect of delocalizing the HOMO more evenly over the core and the LUMO over the phenyl surfactants. The band edge orbitals for $[CdS]_{10}$−Ph are similar in character to those of $[CdS]_{32}$−Ph although more strongly hybridized over the phenyl ligands (see the Supporting Information); they tend to be more evenly delocalized over the whole nanocrystal compared to $[CdS]_{32}$−Ph.

The key mechanisms affecting the electronic structure can be deconvolved in terms of a variety of effects, including: quantum confinement, which increases the energy gap with decreasing size; molecular hybridization, which delocalizes some of the states over the ligands; isotropic compression, which changes the energy gap according to the pressure coefficient of bulk ZB; distortions, which break the local symmetry and affect energy levels (lift degeneracies), and charge-carrier localization and electrostatic effects, such as charge redistribution and interfacial dipoles due to ligands. All of these depend on size, ligands, and pressure and can have competing effects. In summary it is found that smaller size, higher pressure, and phenyl ligands result in more delocalized edge orbitals and more pronounced structural disorder, breaking symmetry and lifting orbital degeneracies with consequences for the optical response. These factors are explored in more detail in the Supporting Information.

However, HOMO−LUMO gaps are not the whole story, as strongly allowed transitions can arise from other orbitals, and we thus calculate the low-energy portion of the optical absorption spectra with TDDFT, focusing on the main absorption peak and the physically significant pressure range 0−5 GPa. The oscillator strength of each excitation depends both on symmetry and overlap of orbitals. Distortions and hybridization are therefore key to understanding the absorption spectra. We can disentangle these with first-principles simulations by designing computational experiments, in which we change ligands or freeze distortion of the nanocrystal core. The optical transitions can also be decomposed in terms of the contribution from different single-particle Kohn−Sham orbital pairs to determine their character.

Our calculations reveal an intriguing size and ligand dependence of the absorption spectra with pressure as evident in Figure 5a−d. As expected, the smaller nanocrystals have larger absorption energies; however, for both sizes, as the nanocrystals progressively deform upon a pressure increase of up to 5 GPa, the main absorption peak is systematically blue-shifted for the hydrogen-terminated nanocrystals, while it is red-shifted for the phenyl-terminated ones.

In detail, for $[CdS]_{32}$−H, the main absorption peak retains its oscillator strength between 0 and 5 GPa and is shifted up in energy with pressure with the same pressure coefficient as the HOMO−LUMO gap. Indeed analysis of $[CdS]_{32}$−H at 0 GPa shows that this peak is composed of pure transitions from the near-degenerate HOMO−2−HOMO → LUMO. This is expected considering that the states are delocalized over the whole nanocrystal, which remains highly symmetric. The second feature in the absorption spectrum instead arises from transitions more mixed in character. Analysis of $[CdS]_{32}$−H at 5 GPa reveals equivalent contributions to those at 0 GPa. Results are similar for $[CdS]_{10}$−H, except that the oscillator strengths of the main peak are reduced as pressure is increased due to the distortions breaking the symmetry as opposed to a reduction in electron−hole overlap (the band edge orbitals remain delocalized over the whole nanocrystal). The effect of degeneracy-lifting due to deformation is evident when comparing the absorption spectra obtained with the full structural relaxation with those based on isotropic scaling of coordinate neglecting distortions (Figure 5c,e).

Interestingly, for $[CdS]_{32}$−Ph at 0 GPa, the main peak is mostly due to HOMO−7−HOMO−5 → LUMO. The oscillator strengths of transitions due to HOMO−2−HOMO → LUMO are suppressed due to hybridization over ligands reducing electron−hole overlap. The second feature is relatively broad and arises from multiple transitions that are mixed in character. At 5 GPa, the main peak is due to HOMO−2−HOMO → LUMO, which gains in oscillator strength as the orbitals delocalize more over the core of the nanocrystal and the electron−hole overlap increases. Again, the oscillator strength of the main peak gradually reduces with increasing pressure again, which can be interpreted as a combined effect of disorder and hybridization. We attempt to disentangle these by replacing the methyl and phenyl groups of $[CdS]_{32}$−Ph relaxed at 5 GPa with H atoms and relaxing these while keeping all other atoms fixed (Figure 5g); the corresponding spectra indicate that, while both effects account for the reduction of the main peak energy at 5 GPa, it is mostly hybridization that reduces its oscillator strength.

For $[CdS]_{10}$−Ph, at 0 GPa, the transition HOMO−2−HOMO → LUMO is again suppressed, and the main peak arises from multiple transitions that are mixed in character. In Figure 5f, we replace methyl and phenyl groups with H atoms

DOI: 10.1021/acs.nanolett.6b04461
Nano Lett. 2017, 17, 1042−1048

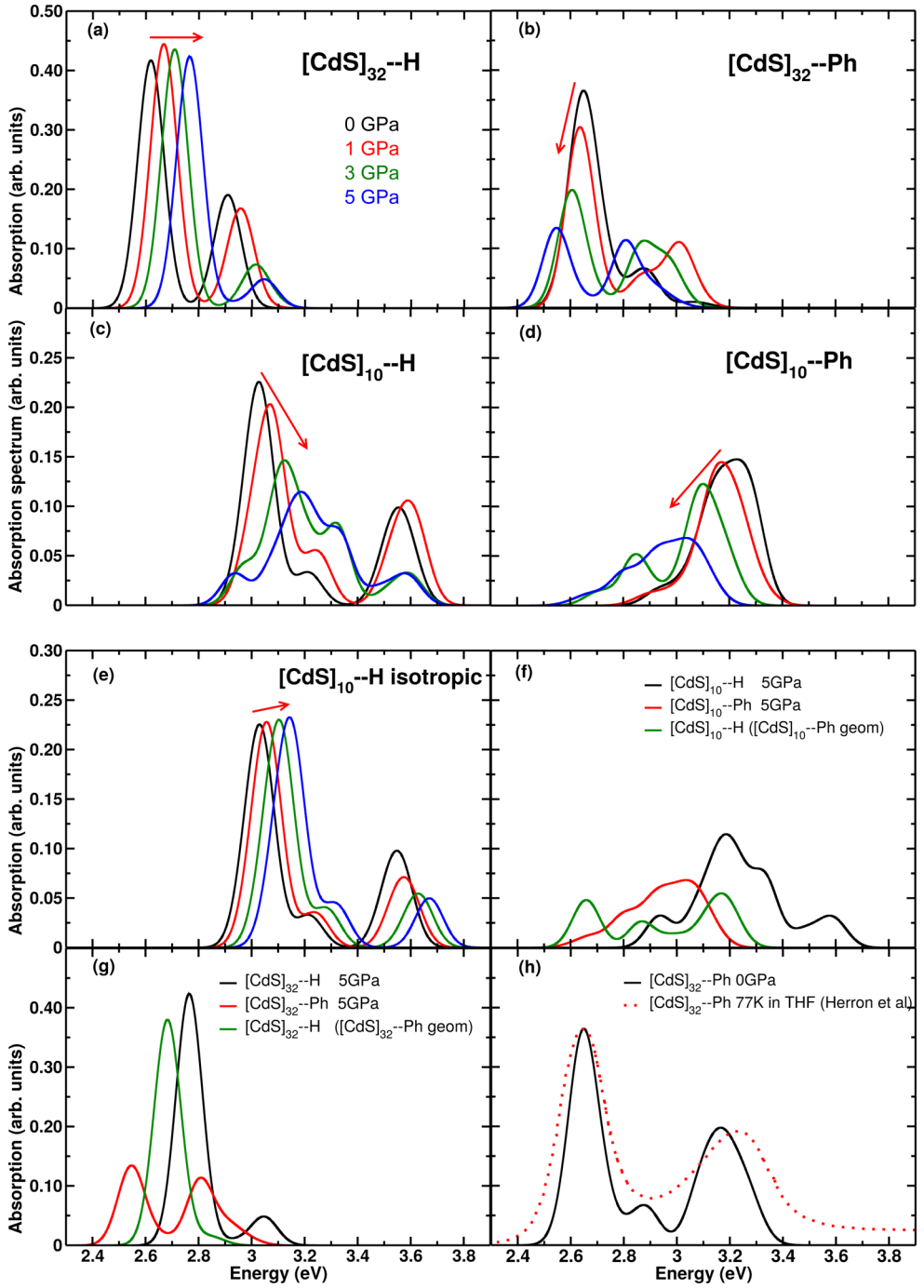

Figure 5. Top four panels: TDDFT optical absorption spectra at various pressures for: (a) $[CdS]_{32}$−H; (b) $[CdS]_{32}$−Ph; (c) $[CdS]_{10}$−H; and (d) $[CdS]_{10}$−Ph. Arrows indicate trends as pressure is increased. Bottom four panels: TDDFT optical absorption spectra for: (e) $[CdS]_{10}$−H mimicking compression by an isotropic scaling of coordinates; (f) $[CdS]_{10}$−H, $[CdS]_{10}$−Ph and $[CdS]_{10}$−H with the same distorted core as $[CdS]_{10}$−Ph at 5 GPa; (g) $[CdS]_{32}$−H, $[CdS]_{32}$−Ph and $[CdS]_{32}$−H with the same distorted core as $[CdS]_{32}$−Ph at 5 GPa; and (h) $[CdS]_{32}$−Ph at 0 GPa converged up to 3.6 eV with a comparison to experimental data by Herron et al.[21] for $Cd_{32}S_{14}(SC_6H_5)_{36}(DMF)_4$ in tetrahydrofuran (THF) at 77 K, red-shifted by 0.75 eV.

while keeping core atoms in positions as in the $[CdS]_{10}$−Ph model at 5 GPa. Hybridization does not significantly alter the energy of the main peak onset, as the valence band edge states are delocalized over the whole nanocrystal in both cases but does suppress its oscillator strength considerably. The main peak is broadened and suppressed with pressure due to the degeneracy-lifting resulting from distortions.

To validate our computational protocol, in Figure 5h, we compare the simulated absorption spectra of $[CdS]_{32}$−Ph, calculated by including additional transitions so as to resolve the spectrum up to 3.6 eV, to the experimental spectrum for $Cd_{32}S_{14}(SC_6H_5)_{36}(DMF)_4$ dissolved in tetrahydrofuran (THF) at 77 K.[21] The TDDFT spectrum is able to qualitatively capture the main absorption features observed in the experiment. While the absolute peak positions are underestimated by ∼0.75 eV compared to the result from the experiment, as expected with LDA, their relative separation of 0.52 eV is in good agreement with the experimental value of 0.57 eV. We note that explicit

DOI: 10.1021/acs.nanolett.6b04461
Nano Lett. 2017, 17, 1042−1048

and dielectric solvent effects have been neglected in our calculations and their screening properties may change the energy levels of band-edge orbitals (especially hybridized ones) with significant effects on the absorption spectra.[38,39] We do, however, expect this effect to be limited in the case of a mildly polar solvent such as THF (static dielectric constant of 7.6).

In summary, in this work, we have for the first time combined a range of state-of-the-art DFT techniques, including the PAW formalism, the electronic-enthalpy scheme for finite systems under pressure, and TDDFT, within a linear-scaling framework to explore the piezochromic properties of CdS nanocrystals of experimentally relevant size. We have worked in a size regime in which surface effects are significant, while for much-larger nanocrystals, a bulk-like response is likely to dominate, and we have selected systems with the same shape, which is a variable not addressed in the present study. The overall picture emerging is that of a strong quantitative and qualitative dependence of optoelectronic response with pressure depending on size and ligands, which we have disentangled with the aid of computational experiments. We have demonstrated that the selected prototypical nanocrystals do not behave as merely passivated pieces of bulk with an elastic response dictated purely by the bulk modulus but undergo significant pressure-induced structural deformations, which depend on size and surface chemistry in a complex fashion, with the smaller nanocrystals undergoing more severe deformations. These, in turn, affect the details of the electronic and optical properties. We have shown the peculiar behavior under pressure of the HOMO−LUMO gap of the investigated nanocrystals in comparison with the bulk and the influence of the ligands on the edge orbitals. Specifically, the variation of the HOMO−LUMO gap with pressure is affected by two competing processes: a bulk-like linear increase due to compression and ligand-induced distortions and hybridization of the frontier orbitals. We have revealed that increased pressure in a deformation regime induces a blue-shift in the main absorption peak of the hydrogen-terminated nanocrystals but a red-shift in the phenyl-capped ones and rationalized the effects of symmetry-breaking deformation and ligand-induced hybridization on the peak positions and oscillator strengths. In fact the frontier orbitals strongly hybridize due to the phenyl ligands, and, as pressure is increased, the main absorption peak, which at zero pressure involves deeper hole orbitals, regains a frontier orbital character, resulting in the observed red shift for the phenyl-capped CdS systems.

Our theoretical framework provides results in good agreement with the available experimental data and paves the way toward the study of complex nanosystems of realistic size and of experimental and industrial interest, in which the interplay between different mechanisms on the electronic, optical, and mechanical properties play a crucial role under operating conditions such as applied pressure.

■ ASSOCIATED CONTENT

Supporting Information

The Supporting Information is available free of charge on the ACS Publications website at DOI: 10.1021/acs.nanolett.6b04461.

Computational details on ONETEP and TDDFT benchmarking tests and detailed analysis of structural distortions and electronic properties with pressure. (PDF)

■ AUTHOR INFORMATION

Corresponding Author

*E-mail: carla.molteni@kcl.ac.uk.

ORCID

Carla Molteni: 0000-0002-0402-2376

Notes

The authors declare no competing financial interest.

■ ACKNOWLEDGMENTS

We thank Dr Andrei Sapelkin (Queen Mary University of London) for useful discussions and a critical reading of the manuscript. We are grateful for the computing resources provided by the Imperial College London High Performance Computing Service and the HECToR/ARCHER UK supercomputer facility (EPSRC Grant No. EP/F037457/1 and EP/K013831/1). N.R.C.C. was supported through a studentship in the Centre for Doctoral Training on Theory and Simulations of Materials at Imperial College London (EPSRC grant No. EP/G036888/1). N.D.M.H acknowledges the support of EPSRC grant No. EP/G05567X/1 and the Winton Programme for the Physics of Sustainability, and P.D.H that of EPSRC grant EP/J015059/1. The authors confirm that all data underlying the findings in this paper are fully available without restriction and have been deposited to Zenodo (DOI: 10.5281/zenodo.58269).

■ REFERENCES

(1) Alivisatos, A. P. *J. Phys. Chem.* **1996**, *100*, 13226−13239.
(2) Ghosh, M.; Ghosh, S.; Attariani, H.; Momeni, K.; Seibt, M.; Mohan Rao, G. *Nano Lett.* **2016**, *16*, 5969−5974.
(3) Choi, C. L.; Koski, K. J.; Sivasankar, S.; Alivisatos, A. P. *Nano Lett.* **2009**, *9*, 3544−3549.
(4) Choi, C. L.; Koski, K. J.; Olson, A. C.; Alivisatos, A. P. *Proc. Natl. Acad. Sci. U. S. A.* **2010**, *107*, 21306−21310.
(5) Boles, M. A.; Ling, D.; Hyeon, T.; Talapin, D. V. *Nat. Mater.* **2016**, *15*, 141−153.
(6) Tan, Y.; Jin, S.; Hamers, R. J. *J. Phys. Chem. C* **2013**, *117*, 313−320.
(7) Liu, I.-S.; Lo, H.-H.; Chien, C.-T.; Lin, Y.-Y.; Chen, C.-W.; Chen, Y.-F.; Su, W.-F.; Liou, S.-C. *J. Mater. Chem.* **2008**, *18*, 675−682.
(8) Chen, O.; Yang, Y.; Wang, T.; Wu, H.; Niu, C.; Yang, J.; Cao, Y. C. *J. Am. Chem. Soc.* **2011**, *133*, 17504−17512.
(9) Morgan, B. J.; Madden, P. A. *Nano Lett.* **2004**, *4*, 1581−1585.
(10) Grünwald, M.; Rabani, E.; Dellago, C. *Phys. Rev. Lett.* **2006**, *96*, 255701.
(11) Grünwald, M.; Dellago, C. *Nano Lett.* **2009**, *9*, 2099−2102.
(12) Bealing, C.; Fugallo, G.; Martoňák, R.; Molteni, C. *Phys. Chem. Chem. Phys.* **2010**, *12*, 8542−8550.
(13) Grünwald, M.; Lutker, K.; Alivisatos, A. P.; Rabani, E.; Geissler, P. L. *Nano Lett.* **2013**, *13*, 1367−1372.
(14) Martoňák, R.; Molteni, C.; Parrinello, M. *Phys. Rev. Lett.* **2000**, *84*, 682−685.
(15) Martoňák, R.; Molteni, C.; Parrinello, M. *Comput. Mater. Sci.* **2001**, *20*, 293−299.
(16) Molteni, C.; Martoňák, R.; Parrinello, M. *J. Chem. Phys.* **2001**, *114*, 5358−5365.
(17) Molteni, C.; Martoňák, R. *ChemPhysChem* **2005**, *6*, 1765−1768.
(18) Cococcioni, M.; Mauri, F.; Ceder, G.; Marzari, N. *Phys. Rev. Lett.* **2005**, *94*, 145501.
(19) Corsini, N. R. C.; Greco, A.; Hine, N. D. M.; Molteni, C.; Haynes, P. D. *J. Chem. Phys.* **2013**, *139*, 084117.
(20) Corsini, N. R. C.; Zhang, Y.; Little, W. R.; Karatutlu, A.; Ersoy, O.; Haynes, P. D.; Molteni, C.; Hine, N. D. M.; Hernandez, I.; Gonzalez, J.; Rodriguez, F.; Brazhkin, V. V.; Sapelkin, A. *Nano Lett.* **2015**, *15*, 7334−7340.

DOI: 10.1021/acs.nanolett.6b04461
Nano Lett. 2017, 17, 1042−1048

(21) Herron, N.; Calabrese, J. C.; Farneth, W. E.; Wang, Y. *Science* **1993**, *259*, 1426−1428.
(22) Chen, C.-C.; Herhold, A. B.; Johnson, C. S.; Alivisatos, A. P. *Science* **1997**, *276*, 398−401.
(23) Casida, M.; Huix-Rotllant, M. *Annu. Rev. Phys. Chem.* **2012**, *63*, 287−323.
(24) Skylaris, C.-K.; Haynes, P. D.; Mostofi, A. A.; Payne, M. C. *J. Chem. Phys.* **2005**, *122*, 084119.
(25) Ratcliff, L. E.; Hine, N. D. M.; Haynes, P. D. *Phys. Rev. B: Condens. Matter Mater. Phys.* **2011**, *84*, 165131.
(26) Zuehlsdorff, T. J.; Hine, N. D. M.; Spencer, J. S.; Harrison, N. M.; Riley, D. J.; Haynes, P. D. *J. Chem. Phys.* **2013**, *139*, 064104.
(27) Wilkinson, K. A.; Hine, N. D. M.; Skylaris, C.-K. *J. Chem. Theory Comput.* **2014**, *10*, 4782−4794.
(28) Zuehlsdorff, T.; Hine, N. D. M.; Payne, M. C.; Haynes, P. D. *J. Chem. Phys.* **2015**, *143*, 204107.
(29) Blöchl, P. *Phys. Rev. B: Condens. Matter Mater. Phys.* **1994**, *50*, 17953.
(30) Hine, N. D. M. *J. Phys.: Condens. Matter* **2017**, *29*, 024001.
(31) Perdew, J.; Wang, Y. *Phys. Rev. B: Condens. Matter Mater. Phys.* **1992**, *45*, 13244.
(32) Dreuw, A.; Head-Gordon, M. *J. Am. Chem. Soc.* **2004**, *126*, 4007−4016.
(33) Nguyen, K. A.; Day, P. N.; Pachter, R. *J. Chem. Phys.* **2011**, *135*, 074109.
(34) Kamisaka, H.; Kilina, S. V.; Yamashita, K.; Prezhdo, O. V. *J. Phys. Chem. C* **2008**, *112*, 7800−7808.
(35) Weissker, H.-C.; Ning, N.; Bechstedt, F.; Vach, H. *Phys. Rev. B: Condens. Matter Mater. Phys.* **2011**, *83*, 125413.
(36) Madelung, O.; Rössler, U.; Von der Osten, W. *Intrinsic properties of group IV elements and III-V, II-VI and I-VII compounds*, 1st ed.; Springer-Verlag: Berlin Heidelberg, Germany, 1987.
(37) Kim, D.; Kim, D.-H.; Lee, J.-H.; Grossman, J. C. *Phys. Rev. Lett.* **2013**, *110*, 196802.
(38) Fischer, S. A.; Crotty, A. M.; Kilina, S. V.; Ivanov, S. A.; Tretiak, S. *Nanoscale* **2012**, *4*, 904−914.
(39) Zuehlsdorff, T. J.; Haynes, P. D.; Hanke, F.; Payne, M. C.; Hine, N. D. M. *J. Chem. Theory Comput.* **2016**, *12*, 1853−1861.

DOI: 10.1021/acs.nanolett.6b04461
Nano Lett. 2017, 17, 1042−1048